



**Particulate matter (PM) episodes at a suburban site in Hong Kong: evolution of PM characteristics and role of photochemistry in secondary aerosol formation**

Yi Ming Qin<sup>1</sup>, Yong Jie Li<sup>2,\*</sup>, Hao Wang<sup>3</sup>, Berto Paul Yok Long Lee<sup>3</sup>, Dan Dan Huang<sup>1</sup>, and Chak Keung Chan<sup>1,3,4,\*</sup>

<sup>1</sup>Department of Chemical and Biomolecular Engineering, Hong Kong University of Science and Technology, Hong Kong, China

<sup>2</sup>Faculty of Science and Technology, University of Macau, Taipa, Macau, China

<sup>3</sup>Division of Environment, Hong Kong University of Science and Technology, Hong Kong, China

<sup>4</sup>School of Energy and Environment, City University of Hong Kong, Hong Kong, China

\*To Whom Correspondence Should be Addressed

Chak K. Chan: AC1-G5716, School of Energy and Environment, City University of Hong Kong,

Tat Chee Avenue, Kowloon, Hong Kong, China

Tel: (852) 3442-5593; Fax: (852) 3442-0688

Email: [chak.k.chan@cityu.edu.hk](mailto:chak.k.chan@cityu.edu.hk)

Yong Jie Li: E11-3017, Faculty of Science and Technology, University of Macau, E11, Avenida da Universidade, Taipa, Macau, China

Tel: (853) 8822-4943; Fax: (853) 8822-2426

Email: [yongjieli@umac.mo](mailto:yongjieli@umac.mo)



## 1 Abstract

2 Episodes with high concentrations of particulate matter (PM) across the seasons were investigated during four  
3 one-month campaigns at a suburban site in Hong Kong. High-resolution time-of-flight aerosol mass spectrometer  
4 (HR-ToF-AMS) measurements revealed that both regional transport and secondary formation contributed to high  
5 PM levels during the episodes at this site. Based on distinct meteorological conditions, episodes were categorized  
6 into three types: liquid water content (LWC), solar irradiance (IR), and long-range transport (LRT). Despite the  
7 difference in meteorological conditions, all episodes were characterized by a high fraction of sulfate (45%-56%) and  
8 organics (23%-34%). However, aerosols in LWC episodes were less aged, consisting of the lowest fraction of  
9 secondary organics aerosols (SOA) and the highest fraction of small particles. Large particles mixed internally while  
10 freshly formed small particles mixed externally in LWC episodes. Aerosols in LRT episodes, by contrast, were the  
11 most aged and consisted of the highest proportion of low-volatility oxygenated organic aerosols (LVOOA) and the  
12 lowest proportion of small particles. Both small and large particles mixed externally in LRT episodes. The highest  
13 proportion of semi-volatile oxygenated organic aerosols (SVOOA) and a medium proportion of small particles were  
14 observed in IR episodes. Both small and large particles were likely externally mixed during IR episodes. Unlike in  
15 the other two types of episodes, in IR episodes aerosols experienced the most dramatic size increase and diurnal  
16 variation, with a time lag between SVOOA and LVOOA and a gradual increase in carbon oxidation state ( $\overline{OS}_c \approx$   
17  $2 \times O:C-H:C$ ). Five out of ten episodes were of the IR type, further reflecting the importance of this type of episode.  
18 The evolution of aerosol components in one particular episode of the IR type, which exhibited a clear land-sea  
19 breeze pattern, was examined in detail. Sulfate and SOA due to photochemical aging were very efficiently produced  
20 during the course of six hours. The “fresh” SOA (SVOOA) was initially formed at a higher rate than the “aged”  
21 SOA (LVOOA). The SVOOA transformed to LVOOA at the later stage of photochemical aging. This transformation  
22 was further supported by mass spectral analysis, which showed an increase in the most oxidized ion ( $CO_2^+$ ) and  
23 decreases in moderately oxidized ones ( $C_2H_3O^+$ ,  $C_3H_3O^+$  and  $C_3H_5O^+$ ). By measuring the physical and chemical  
24 properties of PM in a highly time-resolved manner, the current study was able to demonstrate the dynamic and  
25 complex nature of PM transformation during high-PM episodes.



## 26 **1. Introduction**

27 Hong Kong and the rest of the Pearl River Delta (PRD) in China have been battling air pollution episodes as a  
28 result of rapid economic development and urbanization in the region (Ho et al., 2003; Zhong et al., 2013).  
29 Meteorological conditions may govern the regional and long-range transport of air pollutants to Hong Kong. For  
30 example, northerly winds can bring pollutants from the inland areas to Hong Kong, and have been suggested to be  
31 responsible for regional air pollution events in winter (Fang et al., 1999; Huang et al., 2014b, 2009). The majority of  
32 earlier studies used filter sampling with a low time resolution of hours to days, and so were unable to track the  
33 temporal chemical transformation in high particulate matter (PM) episodes. This limitation has hindered our  
34 understanding of the dynamic nature of PM undergoing rapid chemical transformations. Such chemical  
35 transformation can occur within short time periods (e.g., within a day), and so do other physicochemical properties  
36 such as hygroscopic and optical properties. High-time-resolution chemical characterization techniques, for example  
37 the Aerodyne high-resolution time-of-flight aerosol mass spectrometer (HR-ToF-AMS), offer a temporal resolution  
38 of a few minutes. These techniques can thus provide valuable information on rapid changes in the PM composition,  
39 facilitating more detailed analysis of pollution events (Decarlo et al., 2006). HR-ToF-AMS measurements also give  
40 the size distributions of components (DeCarlo et al., 2008; Lee et al., 2013b). These data can reveal the origin,  
41 formation and atmospheric processing mechanisms of PM (Seinfeld and Pandis, 2006; Shiraiwa et al., 2013), but  
42 they remain under-utilized in most aerosol mass spectrometer (AMS) studies.

43 Secondary formation has been recognized as an important route leading to high PM concentrations worldwide  
44 (Zhang et al., 2015a) and is the main culprit for haze episodes in cities across China (Huang et al., 2014a). Secondary  
45 organic aerosol (SOA) has been shown to dominate over primary organic aerosol (POA) after a few hours of  
46 photochemical aging, for instance, in Mexico City (Decarlo et al., 2010; Volkamer et al., 2006), Pasadena (Hayes et  
47 al., 2013) and Tokyo (Takegawa et al., 2006). Semi-volatile oxygenated organic aerosol (SVOOA), which serves as a  
48 proxy for fresh SOA, has been shown to transform to low-volatility oxygenated organic aerosol (LVOOA), which  
49 serves as a proxy for aged SOA, in laboratory experiments (Alfarra et al., 2012; Jimenez et al., 2009). Such  
50 transformation process may contribute substantially to the accumulation of PM, leading to episodic events that are  
51 frequently observed in the fast-developing city clusters in China (Huang et al., 2012; Zhang et al., 2015b).

52 We conducted four one-month campaigns in each of the four seasons at the Hong Kong University of Science and  
53 Technology (HKUST) Air Quality Research Supersite (AQRS) from May 2011 to February 2012 using an Aerodyne



54 HR-ToF-AMS for non-refractory PM<sub>1</sub> (PM with aerodynamic diameter less than 1 micron). We have previously  
55 examined the general characteristics (Lee et al., 2013a; Li et al., 2013, 2015), seasonal trends (Li et al., 2015), aqueous-  
56 phase process in the formation of oxygenated organics (Lee et al., 2013a; Li et al., 2013, 2015), organic sulfur  
57 compounds (Huang et al., 2015), and particle hygroscopicity (Meng et al., 2014; Yeung et al., 2014). Most of these  
58 studies did not explore in detail the evolution of PM characteristics on the timescale of hours. The current work thus  
59 focuses on high PM episodes lasting a day or several days across the seasons. Specifically, we aim to investigate the  
60 role of local photochemical activity in the formation and evolution of secondary aerosols based on the real-time  
61 chemical composition and size distribution data.

62

## 63 2. Experimental Section

### 64 2.1. Sampling Site and Measurements

65 The sampling periods were from 25 April to 1 June 2011 (spring), from 1 September to 29 September 2011  
66 (summer), from 28 October to 15 December 2011 (autumn), and from 19 January to 1 March 2012 (winter). HR-ToF-  
67 AMS measurements were conducted at the HKUST AQRS (22°20'N, 114°16'E). The HR-ToF-AMS operating  
68 procedure, data analysis and species determination have been discussed in Lee et al. (2013a), Li et al. (2015) and  
69 Huang et al. (2015). Briefly, the AMS was operated alternatively between the V+PToF combined mode and the W-  
70 mode for 5 min each. A collection efficiency of 0.5 was employed for measurements at this site, where the particles  
71 have overwhelmingly dominant sulfate content (Aiken et al., 2009; Li et al., 2013). Concentrations of methanesulfonic  
72 acid (MSA) and organosulfates (OS) were estimated by combining the V-mode data for total concentrations and the  
73 W-mode data for high-resolution mass spectral analysis for specific ions (Huang et al., 2015). Mass spectra of organic  
74 sulfur compounds were obtained from standards in laboratory experiments to support the W-mode data analysis  
75 (Huang et al., 2015). We further calculated the particle liquid water content (LWC) by applying E-AIM II (Clegg et  
76 al., 1998) to explore the effects of aqueous processing on PM<sub>1</sub> composition. Gaseous species (CO, CO<sub>2</sub>, SO<sub>2</sub>, NO,  
77 NO<sub>2</sub>, and O<sub>3</sub>) were measured with standard gas analyzers (Teledyne API). Volatile organic compounds (VOCs) were  
78 measured by gas chromatography (Synspec GC955). Meteorological parameters were measured by an automatic  
79 weather station mounted on a tower right next to the supersite. Particle hygroscopicity and size distribution  
80 measurements have previously been taken with a HR-ToF-AMS at this site (Cheung et al., 2015; Man et al., 2015;  
81 Meng et al., 2014; Yeung et al., 2014), and direct reference to the resulting publications will be made where necessary.



82 **2.2. Data analysis**

83 **2.2.1. Criteria for an episodic event**

84 The total non-refractory PM<sub>1</sub> (NR-PM<sub>1</sub>) concentration showed little seasonal variation, with monthly averages  
85 ranging from 14.3 to 15.9 µg m<sup>-3</sup> as reported by Li et al. (2015). In this work, we defined episodic events according to  
86 the following criteria: 1) lasting for at least 24 hours; 2) daily NR-PM<sub>1</sub> average mass concentration exceeding 15 µg  
87 m<sup>-3</sup> (overall monthly averaged concentration); and 3) maximum concentration exceeding 30 µg m<sup>-3</sup>. According to  
88 these criteria, 10 episodic events were identified in the campaigns as shown in Figure S1.

89 **2.2.2. Source apportionment**

90 Following the results in Li et al. (2015), 72-hour backward air trajectory analysis and positive matrix factorization  
91 (PMF) analysis were performed. Briefly, the back trajectory analysis was run at an elevation of 300 m using the  
92 HYSPLIT-4.8 (Hybrid Single-Particle Lagrangian Integrated Trajectory) model developed by NOAA/ARL (U.S.  
93 National Oceanic and Air Administration/Air Resources Laboratory). We classified air masses affecting Hong Kong  
94 into long-, medium-, and short-range transport patterns for transport distances of 1000 km, between 500 and 1000 km,  
95 and less than 500 km, respectively (Su et al., 2015).

96 For PMF analysis, a four-factor solution with hydrocarbon-like organic aerosols (HOA), cooking organic aerosols  
97 (COA), SVOOA, and LVOOA was adopted as in Li et al. (2015). During episodic events, HOA and COA contributed  
98 insignificantly (less than 6% and 5% respectively) to total organic aerosol (OA). Since we are interested in SOA  
99 transformation, HOA and COA were combined into one POA factor in the following discussion.

100 **2.2.3. Size distribution**

101 Size distributions of aerosol species are obtained with the HR-ToF-AMS when a set of pre-selected m/z is scanned  
102 as a function of the particle time of flight. We focus on the size distribution analysis of sulfate and organics because  
103 of their overwhelming dominance in NR-PM<sub>1</sub>. The raw 10-min mass-size distributions of organics and sulfate during  
104 the episodic events were averaged over various time periods pertaining to the resolution (e.g. 24 hours, 1 hour). The  
105 average size distributions were then fitted by the peak fitting tool Multipeak Fit V2 provided by Igor Pro (Wavemetrics)  
106 using two log-normal peaks. The peaks were chosen such that the fit residuals were minimized. The two fitted peaks  
107 of the size distributions will hereafter be referred to as the small particle mode and the large particle mode. Fitting  
108 examples can be found in Figure S2. We will focus on the most important fitting parameters: the particle mass-mode



109 diameter (vacuum aerodynamic diameter,  $D_{va}$ ) indicating the shift in particle size and the integrated peak areas of the  
110 small particle mode and the large particle mode indicating the changes in mass concentrations of larger or smaller  
111 particles.

112

#### 113 2.2.4. Photochemical age

114 The photochemical age is useful for studying the extent of photochemical processing in an air mass. One way to  
115 estimate the photochemical age ( $\Delta t$ ) is by the ratio of a less reactive hydrocarbon to a more reactive one (Kleinman,  
116 2003):

$$117 \quad \Delta t = \frac{\ln\left(\frac{C_j}{C_i} * \frac{C_{i0}}{C_{j0}}\right)}{(k_i - k_j)[OH]} \quad (1)$$

118 in which  $C_i$  and  $C_j$  are concentrations of hydrocarbons  $i$  and  $j$  at time  $t$ , whereas  $C_{i0}$  and  $C_{j0}$  are concentrations of  
119 hydrocarbons  $i$  and  $j$  at time 0. The symbols  $k_i$  and  $k_j$  are their respective rates of reaction with hydroxyl radicals (OH).  
120 Hofzumahaus et al. (2009) reported a high average OH concentration of  $15 \times 10^6$  molecules  $\text{cm}^{-3}$  around noon in the  
121 PRD region, much higher than model predictions. Zhou et al. (2014) used an OH concentration of  $5.2 \times 10^6$  molecules  
122  $\text{cm}^{-3}$  in their calculation of photochemical age in the PRD region. Lacking definitive estimates, we used a conservative  
123 OH concentration of  $1.5 \times 10^6$  molecule  $\text{cm}^{-3}$  (Hayes et al., 2013; Mao et al., 2009) for the discussion of oxidation  
124 trends in this study. The ratio of benzene to toluene has been widely used (El Haddad et al., 2013) because of their  
125 similar emission sources and significantly different rates of reaction with OH radicals ( $k_{\text{benzene-OH}} = 1.23 \times 10^{-12}$   $\text{cm}^3$   
126  $\text{molecule}^{-1} \text{s}^{-1}$ ;  $k_{\text{toluene-OH}} = 6.0 \times 10^{-12}$   $\text{cm}^3 \text{molecule}^{-1} \text{s}^{-1}$  at 298K) (Atkinson Roger, 2000). Because toluene reacts more  
127 rapidly with OH radicals than does benzene, it is depleted more quickly, resulting in higher benzene/toluene ratios in  
128 aged air masses. However, the photochemical age can deviate when fresh pollutants are added to an aged air mass.  
129 Since fresh pollutants were insignificant after 10:00 (i.e. no significant peaks of benzene and toluene after 10:00; see  
130 Figure S3), we set the start time at 10:00 for the discussion of photochemical aging.

### 131 3. Results and Discussion

#### 132 3.1. Meteorological conditions and classification of episodes



133 Table 1 summarizes the meteorological conditions, PM<sub>1</sub> concentrations, and the estimated LWC in the 10 high  
134 PM episodes. All of the episodes involved air masses that originated over East Asia from the north, northeast or  
135 northwest of Hong Kong, and swept over part of the PRD region before reaching the site. Seven of the 10 episodes  
136 (E1-E7) were characterized by medium-range trajectories and the other three (E8-E10) by long-range trajectories.  
137 The individual trajectories are shown in Figure S3. E1 and E2 had much lower solar irradiance (IR) but higher LWC  
138 than the other episodes, which distinguished them from the other medium-range transport episodes. Thus, E1 and E2  
139 were categorized as episodes of the LWC type (medium-range transport with high LWC and low IR) and the other  
140 medium-range transport episodes as episodes of the IR type (medium-range transport with high IR and low LWC).  
141 Li et al. (2013) referred to E1 and E2 as foggy episodes, while Li et al. (2013) and Lee et al. (2013a) referred to E3  
142 as a hazy episode. The long-range transport episodes might be less associated with the local site-specific conditions  
143 and were categorized as episodes of the LRT type.

144 High concentrations of PM can have a number of causes, including enhanced primary emissions (Ji et al., 2014),  
145 concentrating effects due to a decrease in the height of the planetary boundary layer (Petäjä et al., 2016), regional  
146 transport (Huang et al., 2009), as well as active secondary formation (Hayes et al., 2013). Local primary emissions  
147 were not very significant at this site, as can be seen from the low contribution of POA (less than 6%) throughout the  
148 whole campaign. Boundary layer dynamics on the high PM days can be a factor affecting PM concentration, but the  
149 effects were likely minimal as the highest concentration was usually observed during the day at higher mixing heights  
150 (Figure S4). Therefore, regional transport and active secondary formation would be the most probable causes for the  
151 episodic events of high PM concentrations at this suburban site. More detailed meteorological conditions with  
152 chemical characteristics in each episode can be found in Figure S4.

### 153 3.2. Chemical characteristics of high PM episodes

154 Figure 1 shows the chemical constituents of NR-PM<sub>1</sub> in the three types of episodes. It is apparent that sulfate  
155 dominated in all types of episodes. In Hong Kong, sulfate is largely regarded as a major regional pollutant with little  
156 spatial variability, as in the rest of the PRD (Hagler et al., 2006; LOUIE et al., 2005). Nitrate contributed less than 4%  
157 in LWC episodes and IR episodes, but more than 7% in LRT episodes. As LRT episodes occurred in wintertime, the  
158 higher nitrate concentration was likely driven by gas-particle partitioning of ammonium nitrate to the particle at low  
159 temperatures (Seinfeld and Pandis, 2006). Using the PMF-resolved SVOOA and LVOOA as proxies for fresh and



160 aged SOA respectively (Zhang et al., 2011), more details of OA can be revealed. SVOOA had higher contributions in  
161 IR episodes, while LVOOA contributed roughly twice as much as SVOOA did in LRT episodes, because the air mass  
162 was already quite aged when reached the site. LVOOA and SVOOA made similar contributions in LWC episodes.

163 Figure 2 shows the diurnal variations of the NR-PM<sub>1</sub> species, PMF-resolved organic factors, as well as O<sub>x</sub> (O<sub>3</sub>+NO<sub>2</sub>)  
164 in these three types of episodes. SVOOA and LVOOA as well as O<sub>x</sub> increased during the day in IR episodes, with a  
165 time lag between SVOOA and LVOOA. A similar time lag was also observed between SVOOA and LVOOA in the  
166 Yangtze River Delta (YRD), another fast developing region of China (Huang et al., 2012). These delays may be the  
167 result of conversions from fresh SVOOA to aged LVOOA in the afternoon. We explore such a possibility in Section  
168 3.6. SVOOA and LVOOA both exhibit flat diurnal patterns in LWC episodes and LRT episodes.

169 Elemental analysis of OA (ratios of H:C, O:C, N:C, S:C and OM:OC) from the high resolution mass spectra  
170 provides useful information to assess OA evolution. Recently, Canagaratna et al. (2015) used an updated (Improved-  
171 Ambient) method to estimate O:C and H:C ratios, and reported 27% higher O:C ratios and 11% higher H:C ratios than  
172 those estimated using the original (Aiken-Ambient) method. Recalculating the elemental ratios for the September  
173 dataset using the updated method shows little difference from those obtained by simply applying the respective factors  
174 of 1.27 and 1.11 to the O:C and H:C ratios (Figure S5). Hence, the O:C and H:C ratios in this study were corrected by  
175 factors of 1.27 and 1.11, respectively, with Aiken-Ambient values reported in our previous studies. In the Van  
176 Krevelen diagram (Heald et al., 2010; Ng et al., 2011) shown in Figure 3a, data points for LWC episodes (blue) fall  
177 into a lower O:C region than do the data points for IR (red) and LRT episodes (green). Even though data points for IR  
178 episodes and LRT episodes have similar slopes and intercepts in the Van Krevelen diagram, data points for IR episodes  
179 had a much wider spread. These trends are also reflected in the diurnal patterns of carbon oxidation state ( $\overline{\text{OS}}_c \approx 2 \times \text{O:C}$ -  
180 H:C) (Kroll et al., 2011) in Figure 3b. The  $\overline{\text{OS}}_c$  diurnal pattern in LRT episodes was relatively flat, suggesting that  
181 oxidized organics were mostly transported to the site with minor in-situ oxidation. The  $\overline{\text{OS}}_c$  in IR episodes gradually  
182 increased from 09:00 until 15:00. Similar trends were observed for O<sub>x</sub>, LVOOA and to a less extent, SVOOA. With  
183 all these combined, we believe that the local photochemical processing of OA was more likely at play in IR episodes  
184 than the long-range transport of processed aerosols.

185

186 **3.3. Size distributions of sulfate and organics**



187 Figure 4 shows the peak fitting results of the type-averaged size distributions of organics and sulfate mass. The  
188 mass-mode diameters ( $D_{va}$ ) for both the small and large modes of organics and sulfate did not differ considerably  
189 across the episode types (smaller than 5% differences). Within each type of episode, sulfate had a smaller portion of  
190 small particle mode than organics did, indicating that sulfate was mostly aged while local activities resulted in some  
191 fresh emissions of organics. LWC episodes had the largest small mode contribution and LRT episodes had the smallest,  
192 providing additional support that particles were more aged and large particles dominated in LRT episodes while the  
193 proportion of fresher small particles was higher in LWC and IR episodes due to stronger local influences.

194 Various studies have analyzed the particle mixing state based on single-particle instruments such as the aerosol  
195 time-of-flight mass spectrometer (Healy et al., 2013, 2014; Yang et al., 2012) and the single-particle aerosol mass  
196 spectrometer (Wang et al., 2015). Particle mixing state can also be inferred from particle size information obtained  
197 with the AMS. The large mode diameters of organics and sulfate (Pearson's R value equals to 0.7) were strongly  
198 correlated with a slope close to unity in LWC episodes (Figure 5), suggesting that organics and sulfate are likely  
199 internally mixed in large particles. This internal mixing may occur during the process of local aqueous oxidation,  
200 which has been thoroughly discussed in Li et al. (2013). In IR episodes, during which local photochemical oxidation  
201 may have a more obvious influence, larger particles do not mix well internally (poor correlation between the large  
202 mode diameters of organics and sulfate with  $R_{pr} = 0.2$ ). As discussed in Section 3.2, in IR episodes, organics showed  
203 a clear noontime peak associated with local photochemical activities while sulfate was still mainly a regional pollutant.  
204 As a result, large particles of organics and sulfates were very likely externally mixed during IR episodes. Good  
205 correlation ( $R_{pr} = 0.7$ ) with a large deviation of the slope from unity (slope = 0.5) was observed in LRT episodes. As  
206 long-range transport is the dominant process causing high PM levels during LRT episodes, organics and sulfate would  
207 be brought to the site together, so their large mode diameters tend to be strongly correlated. However, they may have  
208 different origins and may also have undergone different aging processes during the course of long-range transport,  
209 and thus they would have different mode diameters. The correlations between the small mode diameters of organics  
210 and sulfate were notably weaker, with  $R_{pr}=0.5$  in LWC episodes,  $R_{pr}=0.2$  in IR episodes, and  $R_{pr}=0.2$  in LRT episodes,  
211 suggesting that freshly formed small particles mixed externally.

212



213 Figure 6 shows that, in the two LWC episodes, the size variations for both the small and large modes were less  
214 obvious: -2.5% for organics small mode, +8.1% for organics large mode, +1.6% for sulfate small mode, and -3% for  
215 sulfate large mode from start to end as shown in the figure. By contrast, the size variations in the IR episodes were  
216 much more drastic: +51.3% for organics small mode, +40.5% for organics large mode, +45.4% for sulfate small mode,  
217 and +35.9% for sulfate large mode. Furthermore, particle sizes usually increased more rapidly during the days before  
218 the IR episodes (days shaded in blue in Figure 6) than during the actual episodes (days shaded in orange). Since the  
219 particles were fresher and smaller during the days before episodes, they grew more rapidly as gas phase semi-volatile  
220 components condensed onto the particles. Moreover, the number concentrations of the pre-existing particles (acting  
221 as condensation nuclei) were lower before than during the episodes, rendering more rapid size increases before the  
222 episodes.

223

### 224 3.4. Frequency of high PM<sub>1</sub> episodes

225 As is apparent from Table 1, the occurrence of different types of episodes exhibits a seasonal trend. LWC episodes  
226 occurred only in spring and LRT episodes only in winter, while IR episodes took place in spring, summer and autumn.  
227 This result is consistent with previous results (Huang et al., 2009) in that the frequency of high PM days in Hong Kong  
228 had a strong seasonal variation. In winter, the overwhelming northerly wind brings pollutants via long-range transport  
229 (Fang et al., 1999). In spring, foggy days with high PM levels are common due to the moisture-laden air masses  
230 coming in from the sea and aqueous-phase processing of particulate species (Li et al., 2013). In summer, however,  
231 hazy days are mainly due to high photochemical activities in this subtropical area, resulting in the formation of  
232 secondary aerosols (Hu et al., 2008; Zhou et al., 2014).

### 233 3.5. Local photochemical formation and evolution of PM: A case study

#### 234 3.5.1. Time series of species during the local photochemical episode

235 Because of the high frequency of occurrence of IR episodes, we chose one typical IR episode (E4) to examine the  
236 evolution of the aerosols with photochemical oxidation. This particular episode (E4) was under the influence of a clear  
237 land-sea breeze pattern with weak winds (Figure 7), a typical meteorological phenomenon that affects air pollution  
238 dynamics at this coastal city (Lee et al., 2013a). Despite the fact that the 72-hour air mass back trajectories (with  
239 arriving height of 300 m) reflected medium-range transport, the surface air was quite stagnant as shown by wind speed



240 data collected from the ground station. As can be seen from Figure 7, the maximum wind speed was less than  $2 \text{ m s}^{-1}$   
241 while the average wind speed was approximately  $0.5 \text{ m s}^{-1}$ . The wind direction changed from northerly to easterly  
242 between 06:00 and 10:00 and remained easterly until 20:00, when it changed clockwise from easterly back to northerly.  
243 Under such conditions, local photochemical activities can lead to effective production and accumulation of air  
244 pollutants. Time series of organics, sulfate, ammonium, nitrate, MSA, OS, PMF-resolved organic factors, some  
245 gaseous species, as well as meteorological parameters were analyzed. Most NR-PM<sub>1</sub> species showed clear diurnal  
246 variations. Figure 7 shows that organics increased from a roughly constant concentration of  $10 \mu\text{g m}^{-3}$  at night until  
247 09:00 to its highest concentration of  $16.6 \mu\text{g m}^{-3}$  at 13:00, while sulfate showed a mild increase at 06:00 and then a  
248 sharp increase at 10:30 to reach its highest concentration of  $17.4 \mu\text{g m}^{-3}$  at 16:00. They were overall consistent with  
249 the increasing trend of irradiance, an indicator of photochemical activities, in the afternoon. Nitrate concentration was  
250 high ( $2.5 \mu\text{g m}^{-3}$ ) in the morning and started to decrease from 12:30 onwards to reach  $0.3 \mu\text{g m}^{-3}$  by 16:00, likely  
251 attributable to vertical dilution due to a rise in the height of the planetary boundary layer, or alternatively evaporation  
252 of ammonium nitrate at higher temperatures and lower RH values (Seinfeld and Pandis, 2006). Wind direction started  
253 to change at 20:00, when all the NR-PM<sub>1</sub> species were at their lowest concentrations. POA concentration increased  
254 from  $2.5 \mu\text{g m}^{-3}$  at 00:00 to about  $5 \mu\text{g m}^{-3}$  at 06:00, which might be due to the lowering of the planetary boundary  
255 layer. Conversely, expansion of the boundary layer early in the morning could help disperse the POA. The increase in  
256 LVOOA lagged behind that in SVOOA. Starting from 06:00, SVOOA concentration increased rapidly and peaked at  
257 approximately 13:00, coinciding with the IR peak, possibly due to fresh SOA formation. LVOOA gradually increased  
258 from 12:00 and peaked at 14:00, similar to sulfate. The time lag suggests that some conversion from fresh to aged  
259 SOA might have occurred in the afternoon. Evaporation at the elevated temperature of  $30^\circ\text{C}$  throughout the afternoon  
260 might also have led to the decrease in SVOOA, as with nitrate. The diurnal variation of MSA shows a noontime peak,  
261 consistent with the trend of irradiance. In contrast, OS did not show a clear noontime peak, since OS at this site were  
262 likely affected by inland transportation (Huang et al., 2015).

### 263 3.5.2. Changes in size distribution

264 As shown Figure 8, before 06:00, the size distributions of sulfate and organics were both dominated by a mass  
265 mode diameter of 500 to 600 nm. During 06:00-09:00, a shoulder at 200 nm appeared in the size distribution of sulfate  
266 and in that of organics, indicating some fresh sulfate and organics were formed or emitted (possibly POA). As  
267 photochemical reactions proceeded (09:00-18:00), the shoulder of  $D_{\text{va}}$  at 200 nm became weaker and the size



268 distributions shifted to the larger end. It should be noted that during the whole aging process, the size distributions of  
269 organics were broader than those of sulfate since organics were a mixture of numerous constituents from different  
270 primary sources and reaction products formed via different atmospheric processes. The shifts in size distribution  
271 suggest that secondary aerosol particles with sulfate and organics aged gradually and grew into larger particles.

### 272 3.5.3. Photochemical production of secondary species

273 We examine the daytime photochemical activity during E4 by looking at the SO<sub>2</sub> oxidation and changes in the  
274 degree of oxygenation of particulate organics. The sulfur oxidation ratio (SOR) has been used to evaluate the extent  
275 of atmospheric oxidation of SO<sub>2</sub> to sulfate (Squizzato et al., 2013; Wang et al., 2005). Figure 9c shows the increase in  
276 SOR from 0.2 at 9:00 to 0.7 at 18:00, indicating an efficient conversion from SO<sub>2</sub> to sulfate during daytime in this  
277 episode. Figure 9b shows that the  $\overline{\text{OS}}_c$  increased sharply near 11:00.  $\overline{\text{OS}}_c$  was high after 18:00 because most of the  
278 organics in PM had been converted to highly oxidized organic compounds during the aging process. Indeed, during  
279 this period, LVOOA was the dominant OA component (Figure 7). The increases in SOR and  $\overline{\text{OS}}_c$  coincided with the  
280 increase in the ratio of benzene to toluene (Figure 9c). The oxidation of sulfur species and organic species reflects  
281 efficient oxidation during this photochemical episode.

282 To semi-quantitatively evaluate the efficiency of SOA and sulfate formation, the changes in SOA/ $\Delta\text{CO}$ ,  
283 MSA/ $\Delta\text{CO}$ , and sulfate/ $\Delta\text{CO}$  are plotted in Figure 10 as a function of photochemical age from 10:00 to 18:00.  $\Delta\text{CO}$ ,  
284 defined as the measured CO concentration minus the minimum CO concentration (see Figure 7 for the time series of  
285 CO), is assumed to be a conservative tracer of urban combustion emissions. The perturbations of CO concentration  
286 by photochemical formation from VOC or destruction by OH radicals were thought to be negligible over such a short  
287 timescale (less than eight hours) (Griffin et al., 2007). Normalization of species concentrations to the  $\Delta\text{CO}$   
288 concentration is expected to reduce the effect of dilution (Hayes et al., 2013; Zhou et al., 2014).

289 From 10:00 to 18:00, sulfate/ $\Delta\text{CO}$  increased by a factor of 7-8 as photochemical activity increased on a timescale  
290 of approximately 6 h, with a formation rate (indicated by the slope of species/ $\Delta\text{CO}$  vs. photochemical age) of  
291 approximately 48  $\mu\text{g m}^{-3} \text{ppm}^{-1} \text{h}^{-1}$ . MSA/ $\Delta\text{CO}$  also increased by a factor of approximately 3 at a rate of 0.05  $\mu\text{g m}^{-3}$   
292  $\text{ppm}^{-1} \text{h}^{-1}$  during photochemical aging. The good correlation of MSA production with the photochemical age suggests  
293 that MSA originated from the reaction of gaseous dimethyl sulfide with OH radicals (Barnes et al., 2006). For  
294 comparison, Bardouki et al. (2003) also found that MSA and OH radicals covaried over the northeastern coast of Crete.  
295 As shown in Figure 10c, SOA/ $\Delta\text{CO}$  increased by approximately a factor of 2 with the slope of 7.2  $\mu\text{g m}^{-3} \text{ppm}^{-1} \text{h}^{-1}$



296 (8.07  $\mu\text{g sm}^{-3}\text{ppm}^{-1}\text{h}^{-1}$ ). A shallower slope (approximately 4.0 to 4.5  $\mu\text{g sm}^{-3}\text{ppm}^{-1}\text{h}^{-1}$ ) was observed in Pasadena,  
297 California from May to June (Hayes et al., 2013) while a similar slope (6.18  $\mu\text{g m}^{-3}\text{ppm}^{-1}\text{h}^{-1}$ ) was observed in a  
298 previous study in Hong Kong in August (Zhou et al., 2014). This indicates that the SOA production in Hong Kong  
299 during the local in situ photochemical oxidation in summer is high.

300 More interestingly, SVOOA/ $\Delta\text{CO}$  increased during the first three hours but decreased slightly after 13:00, even as  
301 photochemical age increased. In contrast, LVOOA/ $\Delta\text{CO}$  increased steadily throughout the whole stage. After  
302 photochemical processing for 6 h, LVOOA/ $\Delta\text{CO}$  increased by approximately a factor of 20, from 2.3  $\mu\text{g m}^{-3}\text{ppm}^{-1}$   
303 to 49.4  $\mu\text{g m}^{-3}\text{ppm}^{-1}$ . Even though both SVOOA/ $\Delta\text{CO}$  and LVOOA/ $\Delta\text{CO}$  increased in the first stage, they did so at  
304 slightly different rates, where SVOOA/ $\Delta\text{CO}$  increased faster than LVOOA/ $\Delta\text{CO}$ . This suggests that the production of  
305 SVOOA was more efficient than that of LVOOA in the first stage. However, in the later stage of SOA formation, the  
306 net productions of SVOOA were negative, which indicates that SVOOA may have photochemically converted to  
307 LVOOA. As discussed earlier, the input of POA and VOC was limited to the early morning in our study. SVOOA  
308 was consumed more quickly to form LVOOA than was replenished through further production in the late afternoon.  
309 The situation where limited precursors exist to replenish fresh SOA (even under strong photochemical activity) might  
310 also occur in other non-urban atmospheric environments, and thus may have an implication for OA transformation in  
311 general.

#### 312 3.5.4. Mass spectral evolution

313 Figure 11a shows the evolving organic mass spectra during E4 (corresponding to the period of photochemical aging).  
314 Eight spectra at one-hour intervals from 10:00 to 18:00 are shown from top to bottom. Two changes in the mass spectra  
315 with photochemical processes were apparent: 1) decreases in the signal intensities of relatively high  $m/z$  ions (e.g.,  
316  $m/z$  55, 57, 67, 69, etc.), which indicates greater fragmentation (C-C bond cleavage) with photochemical oxidation;  
317 and 2) increases in the mass concentrations of ions having  $m/z$  values of 28 (mainly  $\text{CO}^+$ ) and 44 (mainly  $\text{CO}_2^+$ ),  
318 which presumably come from aldehyde, ketone and carboxylic acid (Ng et al., 2011). These changes are also reflected  
319 in the relative intensity changes of hydrocarbon-like and oxygen-containing ions such as  $\text{C}_4\text{H}_7^+$ ,  $\text{C}_2\text{H}_3\text{O}^+$  and  $\text{CO}_2^+$   
320 (Figure 11b, c). The fractions of tracers of primary organic aerosols  $\text{C}_3\text{H}_7^+$  ( $m/z$  43),  $\text{C}_4\text{H}_7^+$  ( $m/z$  55) and  $\text{C}_4\text{H}_9^+$  ( $m/z$   
321 57) (Lambe et al., 2012) decreased. On the other hand, ion fractions of  $\text{C}_2\text{H}_3\text{O}^+$  ( $m/z$  43),  $\text{C}_3\text{H}_3\text{O}^+$  ( $m/z$  55) and  $\text{C}_3\text{H}_5\text{O}^+$   
322 ( $m/z$  57) increased until 13:00 (corresponding to the peak of SVOOA), followed by the decrease of these moderately  
323 oxygenated ions. These ions are predominantly from non-acid oxygenates, and are usually associated with fresh SOA.



324 However, The most oxidized ions,  $\text{CO}_2^+$  ( $m/z$  44), which is thought to be the marker of aged SOA, increased  
325 continuously. As a result, the mass spectra, which were initially SVOOA-like, evolved to become LVOOA-like with  
326 increasing photochemical age (Figure 11d). Overall, this spectral analysis indicates increasingly oxidized organics, as  
327 long carbon chains became more functionalized and fragmented after extensive oxidation (Alfarra et al., 2012; Kroll  
328 et al., 2009). Such an observation implies efficient transformation of OA within a few hours of photochemical aging,  
329 a timescale that could be relevant to chemical transport models concerning SOA formation.

#### 330 4. Conclusion

331 High-resolution HR-ToF-AMS measurements were taken during four one-month campaigns in suburban Hong  
332 Kong to illustrate the evolution of high PM episodic events across the seasons. Three types of episodes, medium-  
333 range transport with high particle liquid water content (LWC episodes), medium-range transport with high solar  
334 irradiance (IR episodes), and long-range transport (LRT episodes), were captured based on synoptic meteorological  
335 conditions. Which type of episode occurred depended on the season, with LWC episodes occurring only in spring  
336 and LRT episodes only in winter, while IR episodes took place throughout the year except in winter. Sulfate was the  
337 major constituent of  $\text{NR-PM}_1$  during all episodic events. The contribution of secondary organic species, including  
338 SVOOA and LVOOA, varied across episode types, with more SVOOA in the IR episodes and more LVOOA in the  
339 LRT episodes. Unlike in the other two types of episodes, in IR episodes organics experienced the most dramatic  
340 diurnal variation, with a time lag between SVOOA and LVOOA. This variation was associated with Ox, indicating  
341 the conversions from fresh to aged SOA under photochemical oxidation. Elemental analysis involving the Van  
342 Krevelen diagram and carbon oxidation state ( $\overline{\text{OS}}_c \approx 2 \times \text{O}:\text{C}:\text{H}:\text{C}$ ) further showed that organics in IR were gradually  
343 oxidized.

344 Fitted mass-mode diameters for both the small and the large mode of organics remained roughly constant across  
345 episode types, while sulfate had a constant small mode diameter in all three types of episodes but a slightly  
346 increased large mode diameter in IR episodes. The fraction of small particles decreased from LWC episodes to IR  
347 episodes then to LRT episodes, suggesting that aerosols from long-range transport were more aged and dominated  
348 by large particles while episodes under a greater influence of local processes had a higher proportion of fresher  
349 small particles. Large particles mixed internally only in LWC episodes, and were more likely to mix externally in IR  
350 and LRT episodes. Freshly formed small particles mixed externally in all types of episodes. In IR episodes, aerosols  
351 underwent an obvious size increase, while in LWC episodes, the size increase was much less drastic.



352 Because of the high frequency of IR episodes, we picked one particular IR episode featuring land-sea breeze to  
353 examine in detail the evolution of aerosol components. Photochemical aging led to mode size shifting for sulfate and  
354 organics, indicating particle growth. Increases in the sulfur oxidation ratio and carbon oxidation state were also  
355 observed as the aerosols became more aged, which indicates that secondary inorganic species sulfate and SOA were  
356 very efficiently produced within six hours of photochemical aging. In the earlier stage of aging, “fresh” SOA—  
357 SVOOA—was formed at a higher rate than “aged” SOA—LVOOA. SVOOA clearly transformed to LVOOA at the  
358 later stage of photochemical aging, resulting in a 20-fold increase in LVOOA. This conversion was further supported  
359 by mass spectral analysis, which showed an increase in the most oxidized ion ( $\text{CO}_2^+$ ) and decreases in moderately  
360 oxidized ones ( $\text{C}_2\text{H}_3\text{O}^+$ ,  $\text{C}_3\text{H}_3\text{O}^+$  and  $\text{C}_3\text{H}_5\text{O}^+$ ). With real-time size-resolved chemical composition data, we  
361 demonstrated that aerosol components can transform very efficiently in just a few hours, a process that is essential in  
362 understanding the dynamic nature of aerosol evolution during episodes with high PM concentrations.

### 363 Acknowledgements

364 This work was supported by the Environmental Conservation Fund of Hong Kong (project number ECWW09EG04)  
365 and the Research Grants Council of the Hong Kong Special Administrative Region, China (General Research Fund  
366 600413). Y.J. Li gratefully acknowledges the support from the Start-up Research Grant (SRG2015-00052-FST) of the  
367 University of Macau. The grant from the HKUST Asian Future Leaders Scholarship Program (AFLSP) is also  
368 gratefully acknowledged.

369

370

371

372

373

### 374 References

- 375 Aiken, A. C., Salcedo, D., Cubison, M. J., Huffman, J. A., DeCarlo, P. F., Ulbrich, I. M., Docherty, K. S., Sueper,  
376 D., Kimmel, J. R., Worsnop, D. R., Trimborn, A., Northway, M., Stone, E. A., Schauer, J. J., Volkamer, R. M.,  
377 Fortner, E., de Foy, B., Wang, J., Laskin, A., Shutthanandan, V., Zheng, J., Zhang, R., Gaffney, J., Marley, N. A.,  
378 Paredes-Miranda, G., Arnott, W. P., Molina, L. T., Sosa, G. and Jimenez, J. L.: Mexico City aerosol analysis during  
379 MILAGRO using high resolution aerosol mass spectrometry at the urban supersite (T0) – Part 1: Fine particle  
380 composition and organic source apportionment, Atmos. Chem. Phys., 9(17), 6633–6653, doi:10.5194/acp-9-6633-  
381 2009, 2009.
- 382 Alfarra, M. R., Hamilton, J. F., Wyche, K. P., Good, N., Ward, M. W., Carr, T., Barley, M. H., Monks, P. S., Jenkin,



- 383 M. E., Lewis, A. C. and McFiggans, G. B.: The effect of photochemical ageing and initial precursor concentration  
384 on the composition and hygroscopic properties of  $\beta$ -caryophyllene secondary organic aerosol, Atmos. Chem. Phys.,  
385 12(14), 6417–6436, doi:10.5194/acp-12-6417-2012, 2012.
- 386 Atkinson Roger, J. A.: Atmospheric degradation of volatile methyl-silicon compounds, Environ. Sci. Technol.,  
387 34(10), 1970–1976, doi:10.1021/es9910053, 2000.
- 388 Bardouki, H., Berresheim, H., Vrekoussis, M., Sciare, J., Kouvarakis, G., Oikonomou, K., Schneider, J. and  
389 Mihalopoulos, N.: Gaseous (DMS, MSA, SO<sub>2</sub>, H<sub>2</sub>SO<sub>4</sub> and DMSO) and particulate (sulfate and methanesulfonate)  
390 sulfur species over the northeastern coast of Crete, Atmos. Chem. Phys., 3(5), 1871–1886, doi:10.5194/acp-3-1871-  
391 2003, 2003.
- 392 Barnes, I., Hjorth, J. and Mihalopoulos, N.: Dimethyl sulfide and dimethyl sulfoxide and their oxidation in the  
393 atmosphere, Chem. Rev., 106(3), 940–975, doi:10.1021/cr020529+, 2006.
- 394 Canagaratna, M. R., Jimenez, J. L., Kroll, J. H., Chen, Q., Kessler, S. H., Massoli, P., Hildebrandt Ruiz, L., Fortner,  
395 E., Williams, L. R., Wilson, K. R., Surratt, J. D., Donahue, N. M., Jayne, J. T. and Worsnop, D. R.: Elemental ratio  
396 measurements of organic compounds using aerosol mass spectrometry: characterization, improved calibration, and  
397 implications, Atmos. Chem. Phys., 15(1), 253–272, doi:10.5194/acp-15-253-2015, 2015.
- 398 Cheung, H. H. Y., Yeung, M. C., Li, Y. J., Lee, B. P. and Chan, C. K.: Relative Humidity-Dependent HTDMA  
399 Measurements of Ambient Aerosols at the HKUST Supersite in Hong Kong, China, Aerosol Sci. Technol., 49(8),  
400 643–654, doi:10.1080/02786826.2015.1058482, 2015.
- 401 Clegg, S. L., Brimblecombe, P. and Wexler, A. S.: Thermodynamic Model of the System  $H^+ - NH_4^+ - Na^+ - SO_4^{2-} - NO_3^- - Cl^- - H_2O$  at 298.15 K, J. Phys. Chem. A, 102(12), 2155–2171, doi:10.1021/jp973043j, 1998.
- 403 Decarlo, P. F., Kimmel, J. R., Trimborn, A., Northway, M. J., Jayne, J. T., Aiken, A. C., Gonin, M., Fuhrer, K.,  
404 Horvath, T., Docherty, K. S., Worsnop, D. R. and Jimenez, J. L.: Field-Deployable, High-Resolution, Time-of-  
405 Flight Aerosol Mass Spectrometer, Anal. Chem., 78(24), 8281–8289, doi:8410.1029/2001JD001213, Analytical,  
406 2006.
- 407 DeCarlo, P. F., Dunlea, E. J., Kimmel, J. R., Aiken, A. C., Sueper, D., Crouse, J., Wennberg, P. O., Emmons, L.,  
408 Shinzuka, Y., Clarke, A., Zhou, J., Tomlinson, J., Collins, D. R., Knapp, D., Weinheimer, A. J., Montzka, D. D.,  
409 Campos, T. and Jimenez, J. L.: Fast airborne aerosol size and chemistry measurements above Mexico City and  
410 Central Mexico during the MILAGRO campaign, Atmos. Chem. Phys., 8(14), 4027–4048, doi:10.5194/acp-8-4027-  
411 2008, 2008.
- 412 Decarlo, P. F., Ulbrich, I. M., Crouse, J., De Foy, B., Dunlea, E. J., Aiken, a. C., Knapp, D., Weinheimer, a. J.,  
413 Campos, T., Wennberg, P. O. and Jimenez, J. L.: Investigation of the sources and processing of organic aerosol over  
414 the Central Mexican Plateau from aircraft measurements during MILAGRO, Atmos. Chem. Phys., 10(12), 5257–  
415 5280, doi:10.5194/acp-10-5257-2010, 2010.
- 416 Fang, M., Zheng, M., Wang, F., Chim, K. and Kot, S.: The long-range transport of aerosols from northern China to  
417 Hong Kong - a multi-technique study, Atmos. Environ., 33(11), 1803–1817 [online] Available from:  
418 <http://repository.ust.hk/ir/Record/1783.1-28286> (Accessed 9 November 2015), 1999.
- 419 Griffin, R. J., Chen, J., Carmody, K., Vutukuru, S. and Dabdub, D.: Contribution of gas phase oxidation of volatile  
420 organic compounds to atmospheric carbon monoxide levels in two areas of the United States, J. Geophys. Res.,  
421 112(D10), D10S17, doi:10.1029/2006JD007602, 2007.
- 422 El Haddad, I., D'Anna, B., Temime-Roussel, B., Nicolas, M., Boreave, a., Favez, O., Voisin, D., Sciare, J., George,  
423 C., Jaffrezo, J.-L., Wortham, H. and Marchand, N.: Towards a better understanding of the origins, chemical  
424 composition and aging of oxygenated organic aerosols: case study of a Mediterranean industrialized environment,  
425 Marseille, Atmos. Chem. Phys., 13(15), 7875–7894, doi:10.5194/acp-13-7875-2013, 2013.
- 426 Hagler, G. S. W., Bergin, M. H., Salmon, L. G., Yu, J. Z., Wan, E. C. H., Zheng, M., Zeng, L. M., Kiang, C. S.,  
427 Zhang, Y. H., Lau, A. K. H. and Schauer, J. J.: Source areas and chemical composition of fine particulate matter in  
428 the Pearl River Delta region of China, Atmos. Environ., 40(20), 3802–3815, doi:10.1016/j.atmosenv.2006.02.032,  
429 2006.



- 430 Hayes, P. L., Ortega, a. M., Cubison, M. J., Froyd, K. D., Zhao, Y., Cliff, S. S., Hu, W. W., Toohey, D. W., Flynn,  
 431 J. H., Lefer, B. L., Grossberg, N., Alvarez, S., Rappenglück, B., Taylor, J. W., Allan, J. D., Holloway, J. S., Gilman,  
 432 J. B., Kuster, W. C., De Gouw, J. a., Massoli, P., Zhang, X., Liu, J., Weber, R. J., Corrigan, a. L., Russell, L. M.,  
 433 Isaacman, G., Worton, D. R., Kreisberg, N. M., Goldstein, a. H., Thalman, R., Waxman, E. M., Volkamer, R., Lin,  
 434 Y. H., Surratt, J. D., Kleindienst, T. E., Offenberg, J. H., Dusanter, S., Griffith, S., Stevens, P. S., Brioude, J.,  
 435 Angevine, W. M. and Jimenez, J. L.: Organic aerosol composition and sources in Pasadena, California, during the  
 436 2010 CalNex campaign, *J. Geophys. Res. Atmos.*, 118(16), 9233–9257, doi:10.1002/jgrd.50530, 2013.
- 437 Heald, C. L., Kroll, J. H., Jimenez, J. L., Docherty, K. S., Decarlo, P. F., Aiken, a. C., Chen, Q., Martin, S. T.,  
 438 Farmer, D. K. and Artaxo, P.: A simplified description of the evolution of organic aerosol composition in the  
 439 atmosphere, *Geophys. Res. Lett.*, 37(8), doi:10.1029/2010GL042737, 2010.
- 440 Healy, R. M., Sciare, J., Poulain, L., Crippa, M., Wiedensohler, A., Prévôt, A. S. H., Baltensperger, U., Sarda-  
 441 Estève, R., McGuire, M. L., Jeong, C.-H., McGillicuddy, E., O'Connor, I. P., Sodeau, J. R., Evans, G. J. and  
 442 Wenger, J. C.: Quantitative determination of carbonaceous particle mixing state in Paris using single-particle mass  
 443 spectrometer and aerosol mass spectrometer measurements, *Atmos. Chem. Phys.*, 13(18), 9479–9496,  
 444 doi:10.5194/acp-13-9479-2013, 2013.
- 445 Healy, R. M., Riemer, N., Wenger, J. C., Murphy, M., West, M., Poulain, L., Wiedensohler, A., O'Connor, I. P.,  
 446 McGillicuddy, E., Sodeau, J. R. and Evans, G. J.: Single particle diversity and mixing state measurements, *Atmos.*  
 447 *Chem. Phys.*, 14(12), 6289–6299, doi:10.5194/acp-14-6289-2014, 2014.
- 448 Ho, K. ., Lee, S. ., Chan, C. K., Yu, J. C., Chow, J. C. and Yao, X. .: Characterization of chemical species in PM<sub>2.5</sub>  
 449 and PM<sub>10</sub> aerosols in Hong Kong, *Atmos. Environ.*, 37(1), 31–39, doi:10.1016/S1352-2310(02)00804-X, 2003.
- 450 Hofzumahaus, A., Rohrer, F., Lu, K., Bohn, B., Brauers, T., Chang, C.-C., Fuchs, H., Holland, F., Kita, K., Kondo,  
 451 Y., Li, X., Lou, S., Shao, M., Zeng, L., Wahner, A. and Zhang, Y.: Amplified trace gas removal in the troposphere.,  
 452 *Science*, 324(5935), 1702–1704, doi:10.1126/science.1164566, 2009.
- 453 Hu, D., Bian, Q., Li, T. W. Y., Lau, A. K. H. and Yu, J. Z.: Contributions of isoprene, monoterpenes,  $\beta$ -  
 454 caryophyllene, and toluene to secondary organic aerosols in Hong Kong during the summer of 2006, *J. Geophys.*  
 455 *Res. Atmos.*, 113(22), 1–14, doi:10.1029/2008JD010437, 2008.
- 456 Huang, D. D., Li, Y. J., Lee, B. P. and Chan, C. K.: Analysis of Organic Sulfur Compounds in Atmospheric  
 457 Aerosols at the HKUST Supersite in Hong Kong Using HR-ToF-AMS, *Environ. Sci. Technol.*, 150305134049007,  
 458 doi:10.1021/es5056269, 2015.
- 459 Huang, R.-J., Zhang, Y., Bozzetti, C., Ho, K.-F., Cao, J.-J., Han, Y., Daellenbach, K. R., Slowik, J. G., Platt, S. M.,  
 460 Canonaco, F., Zotter, P., Wolf, R., Pieber, S. M., Bruns, E. a., Crippa, M., Ciarelli, G., Piazzalunga, A.,  
 461 Schwikowski, M., Abbaszade, G., Schnelle-Kreis, J., Zimmermann, R., An, Z., Szidat, S., Baltensperger, U.,  
 462 Haddad, I. El and Prévôt, A. S. H.: High secondary aerosol contribution to particulate pollution during haze events  
 463 in China, *Nature*, doi:10.1038/nature13774, 2014a.
- 464 Huang, X. F., He, L. Y., Xue, L., Sun, T. L., Zeng, L. W., Gong, Z. H., Hu, M. and Zhu, T.: Highly time-resolved  
 465 chemical characterization of atmospheric fine particles during 2010 Shanghai World Expo, *Atmos. Chem. Phys.*,  
 466 12(11), 4897–4907, doi:10.5194/acp-12-4897-2012, 2012.
- 467 Huang, X. H. H., Bian, Q., Ng, W. M., Louie, P. K. K. and Yu, J. Z.: Characterization of PM<sub>2.5</sub> major components  
 468 and source investigation in suburban Hong Kong: A one year monitoring study, *Aerosol Air Qual. Res.*, 14(1), 237–  
 469 250, doi:10.4209/aaqr.2013.01.0020, 2014b.
- 470 Huang, X.-F., Yu, J. Z., Yuan, Z., Lau, A. K. H. and Louie, P. K. K.: Source analysis of high particulate matter days  
 471 in Hong Kong, *Atmos. Environ.*, 43(6), 1196–1203, doi:10.1016/j.atmosenv.2008.10.013, 2009.
- 472 Ji, D., Li, L., Wang, Y., Zhang, J., Cheng, M., Sun, Y., Liu, Z., Wang, L., Tang, G., Hu, B., Chao, N., Wen, T. and  
 473 Miao, H.: The heaviest particulate air-pollution episodes occurred in northern China in January, 2013: Insights  
 474 gained from observation, *Atmos. Environ.*, 92, 546–556, doi:10.1016/j.atmosenv.2014.04.048, 2014.
- 475 Jimenez, J. L., Canagaratna, M. R., Donahue, N. M., Prevot, a S. H., Zhang, Q., Kroll, J. H., DeCarlo, P. F., Allan,  
 476 J. D., Coe, H., Ng, N. L., Aiken, a C., Docherty, K. S., Ulbrich, I. M., Grieshop, a P., Robinson, a L., Duplissy, J.,  
 477 Smith, J. D., Wilson, K. R., Lanz, V. a, Hueglin, C., Sun, Y. L., Tian, J., Laaksonen, a, Raatikainen, T., Rautiainen,



- 478 J., Vaattovaara, P., Ehn, M., Kulmala, M., Tomlinson, J. M., Collins, D. R., Cubison, M. J., Dunlea, E. J., Huffman,  
 479 J. a, Onasch, T. B., Alfarra, M. R., Williams, P. I., Bower, K., Kondo, Y., Schneider, J., Drewnick, F., Borrmann, S.,  
 480 Weimer, S., Demerjian, K., Salcedo, D., Cottrell, L., Griffin, R., Takami, a, Miyoshi, T., Hatakeyama, S., Shimono,  
 481 a, Sun, J. Y., Zhang, Y. M., Dzepina, K., Kimmel, J. R., Sueper, D., Jayne, J. T., Herndon, S. C., Trimborn, a M.,  
 482 Williams, L. R., Wood, E. C., Middlebrook, a M., Kolb, C. E., Baltensperger, U. and Worsnop, D. R.: Evolution of  
 483 organic aerosols in the atmosphere., *Science*, 326(5959), 1525–1529, doi:10.1126/science.1180353, 2009.
- 484 Kleinman, L. I.: Photochemical age determinations in the Phoenix metropolitan area, *J. Geophys. Res.*, 108(D3), 1–  
 485 14, doi:10.1029/2002JD002621, 2003.
- 486 Kleinman, L. I., Daum, P. H., Lee, Y. N., Senum, G. I., Springston, S. R., Wang, J., Berkowitz, C., Hubbe, J.,  
 487 Zaveri, R. a., Brechtel, F. J., Jayne, J., Onasch, T. B. and Worsnop, D.: Aircraft observations of aerosol composition  
 488 and ageing in New England and Mid-Atlantic States during the summer 2002 New England Air Quality Study field  
 489 campaign, *J. Geophys. Res. Atmos.*, 112(9), 1–18, doi:10.1029/2006JD007786, 2007.
- 490 Kroll, J. H., Smith, J. D., Che, D. L., Kessler, S. H., Worsnop, D. R. and Wilson, K. R.: Measurement of  
 491 fragmentation and functionalization pathways in the heterogeneous oxidation of oxidized organic aerosol., *Phys.*  
 492 *Chem. Chem. Phys.*, 11(36), 8005–14, doi:10.1039/b905289e, 2009.
- 493 Kroll, J. H., Donahue, N. M., Jimenez, J. L., Kessler, S. H., Canagaratna, M. R., Wilson, K. R., Altieri, K. E.,  
 494 Mazzoleni, L. R., Wozniak, A. S., Bluhm, H., Mysak, E. R., Smith, J. D., Kolb, C. E. and Worsnop, D. R.: Carbon  
 495 oxidation state as a metric for describing the chemistry of atmospheric organic aerosol., *Nat. Chem.*, 3(2), 133–9,  
 496 doi:10.1038/nchem.948, 2011.
- 497 Lambe, A. T., Onasch, T. B., Croasdale, D. R., Wright, J. P., Martin, A. T., Franklin, J. P., Massoli, P., Kroll, J. H.,  
 498 Canagaratna, M. R., Brune, W. H., Worsnop, D. R. and Davidovits, P.: Transitions from Functionalization to  
 499 Fragmentation Reactions of Laboratory Secondary Organic Aerosol (SOA) Generated from the OH Oxidation of  
 500 Alkane Precursors, *Environ. Sci. Technol.*, 46(10), 5430–5437, doi:Doi 10.1021/Es300274t, 2012.
- 501 Lee, B. P., Li, Y. J., Yu, J. Z., Louie, P. K. K. and Chan, C. K.: Physical and chemical characterization of ambient  
 502 aerosol by HR-ToF-AMS at a suburban site in Hong Kong during springtime 2011, *J. Geophys. Res. Atmos.*,  
 503 118(15), 8625–8639, doi:10.1002/jgrd.50658, 2013a.
- 504 Lee, B. P., Li, Y. J., Flagan, R. C., Lo, C. and Chan, C. K.: Sizing Characterization of the Fast-Mobility Particle  
 505 Sizer (FMPS) Against SMPS and HR-ToF-AMS, *Aerosol Sci. Technol.*, 47(9), 1030–1037,  
 506 doi:10.1080/02786826.2013.810809, 2013b.
- 507 Li, Y. J., Lee, B. Y. L., Yu, J. Z., Ng, N. L. and Chan, C. K.: Evaluating the degree of oxygenation of organic  
 508 aerosol during foggy and hazy days in Hong Kong using high-resolution time-of-flight aerosol mass spectrometry  
 509 (HR-ToF-AMS), *Atmos. Chem. Phys.*, 13(17), 8739–8753, doi:10.5194/acp-13-8739-2013, 2013.
- 510 Li, Y. J., Lee, B. P., Su, L., Fung, J. C. H. and Chan, C. K.: Seasonal characteristics of fine particulate matter (PM)  
 511 based on high-resolution time-of-flight aerosol mass spectrometric (HR-ToF-AMS) measurements at the HKUST  
 512 Supersite in Hong Kong, *Atmos. Chem. Phys.*, 15(1), 37–53, doi:10.5194/acp-15-37-2015, 2015.
- 513 LOUIE, P., WATSON, J., CHOW, J., CHEN, A., SIN, D. and LAU, A.: Seasonal characteristics and regional  
 514 transport of PM in Hong Kong, *Atmos. Environ.*, 39(9), 1695–1710, doi:10.1016/j.atmosenv.2004.11.017, 2005.
- 515 Man, H., Zhu, Y., Ji, F., Yao, X., Lau, N. T., Li, Y., Lee, B. P. and Chan, C. K.: Comparison of daytime and  
 516 nighttime new particle growth at the HKUST supersite in Hong Kong., *Environ. Sci. Technol.*, 49(12), 7170–8,  
 517 doi:10.1021/acs.est.5b02143, 2015.
- 518 Mao, J., Ren, X., Brune, W. H., Olson, J. R., Crawford, J. H., Fried, A., Huey, L. G., Cohen, R. C., Heikes, B.,  
 519 Singh, H. B., Blake, D. R., Sachse, G. W., Diskin, G. S., Hall, S. R. and Shetter, R. E.: Airborne measurement of  
 520 OH reactivity during INTEX-B, *Atmos. Chem. Phys.*, 9(1), 163–173, doi:10.5194/acp-9-163-2009, 2009.
- 521 Meng, J. W., Yeung, M. C., Li, Y. J., Lee, B. Y. L. and Chan, C. K.: Size-resolved cloud condensation nuclei (CCN)  
 522 activity and closure analysis at the HKUST Supersite in Hong Kong, *Atmos. Chem. Phys.*, 14(18), 10267–10282,  
 523 doi:10.5194/acp-14-10267-2014, 2014.
- 524 Mohr, C., DeCarlo, P. F., Heringa, M. F., Chirico, R., Slowik, J. G., Richter, R., Reche, C., Alastuey, A., Querol, X.,



- 525 Seco, R., Peñuelas, J., Jiménez, J. L., Crippa, M., Zimmermann, R., Baltensperger, U. and Prévôt, A. S. H.:  
 526 Identification and quantification of organic aerosol from cooking and other sources in Barcelona using aerosol mass  
 527 spectrometer data, *Atmos. Chem. Phys.*, 12(4), 1649–1665, doi:10.5194/acp-12-1649-2012, 2012.
- 528 Ng, N. L., Canagaratna, M. R., Jimenez, J. L., Chhabra, P. S., Seinfeld, J. H. and Worsnop, D. R.: Changes in  
 529 organic aerosol composition with aging inferred from aerosol mass spectra, *Atmos. Chem. Phys.*, 11(13), 6465–  
 530 6474, doi:10.5194/acp-11-6465-2011, 2011.
- 531 Petäjä, T., Järvi, L., Kerminen, V.-M., Ding, A. J., Sun, J. N., Nie, W., Kujansuu, J., Virkkula, A., Yang, X., Fu, C.  
 532 B., Zilitinkevich, S. and Kulmala, M.: Enhanced air pollution via aerosol-boundary layer feedback in China., *Sci.*  
 533 *Rep.*, 6, 18998, doi:10.1038/srep18998, 2016.
- 534 Seinfeld, J. H. and Pandis, S. N.: *ATMOSPHERIC From Air Pollution to Climate Change SECOND EDITION.*,  
 535 2006.
- 536 Shiraiwa, M., Yee, L. D., Schilling, K. a, Loza, C. L., Craven, J. S., Zuend, A., Ziemann, P. J. and Seinfeld, J. H.:  
 537 Size distribution dynamics reveal particle-phase chemistry in organic aerosol formation., *Proc. Natl. Acad. Sci. U. S.*  
 538 *A.*, 110(29), 11746–50, doi:10.1073/pnas.1307501110, 2013.
- 539 Squizzato, S., Masiol, M., Brunelli, a., Pistollato, S., Tarabotti, E., Rampazzo, G. and Pavoni, B.: Factors  
 540 determining the formation of secondary inorganic aerosol: A case study in the Po Valley (Italy), *Atmos. Chem.*  
 541 *Phys.*, 13(4), 1927–1939, doi:10.5194/acp-13-1927-2013, 2013.
- 542 Su, L., Yuan, Z., Fung, J. C. H. and Lau, A. K. H.: A comparison of HYSPLIT backward trajectories generated from  
 543 two GDAS datasets, *Sci. Total Environ.*, 506-507, 527–537, doi:10.1016/j.scitotenv.2014.11.072, 2015.
- 544 Takegawa, N., Miyakawa, T., Kondo, Y., Blake, D. R., Kanaya, Y., Koike, M., Fukuda, M., Komazaki, Y.,  
 545 Miyazaki, Y., Shimono, a. and Takeuchi, T.: Evolution of submicron organic aerosol in polluted air exported from  
 546 Tokyo, *Geophys. Res. Lett.*, 33(15), 3–7, doi:10.1029/2006GL025815, 2006.
- 547 Volkamer, R., Jimenez, J. L., San Martini, F., Dzepina, K., Zhang, Q., Salcedo, D., Molina, L. T., Worsnop, D. R.  
 548 and Molina, M. J.: Secondary organic aerosol formation from anthropogenic air pollution: Rapid and higher than  
 549 expected, *Geophys. Res. Lett.*, 33(17), L17811, doi:10.1029/2006GL026899, 2006.
- 550 Wang, H., Zhu, B., Zhang, Z., An, J. and Shen, L.: Mixing state of individual carbonaceous particles during a severe  
 551 haze episode in January 2013, Nanjing, China, *Particuology*, 20, 16–23, doi:10.1016/j.partic.2014.06.013, 2015.
- 552 Wang, Y., Zhuang, G., Tang, A., Yuan, H., Sun, Y., Chen, S. and Zheng, A.: The ion chemistry and the source of  
 553 PM<sub>2.5</sub> aerosol in Beijing, *Atmos. Environ.*, 39(21), 3771–3784, doi:10.1016/j.atmosenv.2005.03.013, 2005.
- 554 Yang, F., Chen, H., Du, J., Yang, X., Gao, S., Chen, J. and Geng, F.: Evolution of the mixing state of fine aerosols  
 555 during haze events in Shanghai, *Atmos. Res.*, 104-105, 193–201, doi:10.1016/j.atmosres.2011.10.005, 2012.
- 556 Yeung, M. C., Lee, B. P., Li, Y. J. and Chan, C. K.: Simultaneous HTDMA and HR-ToF-AMS measurements at the  
 557 HKUST Supersite in Hong Kong in 2011, *J. Geophys. Res. Atmos.*, 119(16), 9864–9883,  
 558 doi:10.1002/2013JD021146, 2014.
- 559 Zhang, Q., Jimenez, J. L., Canagaratna, M. R., Ulbrich, I. M., Ng, N. L., Worsnop, D. R. and Sun, Y.:  
 560 Understanding atmospheric organic aerosols via factor analysis of aerosol mass spectrometry: A review, *Anal.*  
 561 *Bioanal. Chem.*, 401(10), 3045–3067, doi:10.1007/s00216-011-5355-y, 2011.
- 562 Zhang, R., Wang, G., Guo, S., Zamora, M. L., Ying, Q., Lin, Y., Wang, W., Hu, M. and Wang, Y.: Formation of  
 563 Urban Fine Particulate Matter, *Chem. Rev.*, 115(10), 3803–3855, doi:10.1021/acs.chemrev.5b00067, 2015a.
- 564 Zhang, Y. W., Zhang, X. Y., Zhang, Y. M., Shen, X. J., Sun, J. Y., Ma, Q. L., Yu, X. M., Zhu, J. L., Zhang, L. and  
 565 Che, H. C.: Significant concentration changes of chemical components of PM<sub>1</sub> in the Yangtze River Delta area of  
 566 China and the implications for the formation mechanism of heavy haze-fog pollution., *Sci. Total Environ.*, 538, 7–  
 567 15, doi:10.1016/j.scitotenv.2015.06.104, 2015b.
- 568 Zhong, L., Louie, P. K. K., Zheng, J., Yuan, Z., Yue, D., Ho, J. W. K. and Lau, A. K. H.: Science–policy interplay:  
 569 Air quality management in the Pearl River Delta region and Hong Kong, *Atmos. Environ.*, 76, 3–10,  
 570 doi:10.1016/j.atmosenv.2013.03.012, 2013.



571 Zhou, S., Wang, T., Wang, Z., Li, W., Xu, Z., Wang, X., Yuan, C., Poon, C. N., Louie, P. K. K., Luk, C. W. Y. and  
572 Wang, W.: Photochemical evolution of organic aerosols observed in urban plumes from Hong Kong and the Pearl  
573 River Delta of China, Atmos. Environ., 88, 219–229, doi:10.1016/j.atmosenv.2014.01.032, 2014.

574



Tables:

Table 1 Synopsis of meteorological conditions of high PM episodes

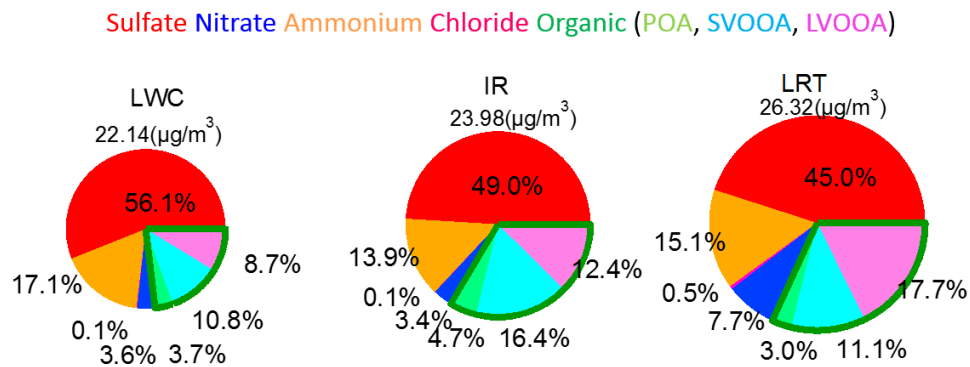
Episode	Season	Date	Air mass origin	Wind speed (m s <sup>-1</sup> )	Solar Irradiance (w m <sup>-2</sup> )	Liquid water content (µg m <sup>-3</sup> )	PM <sub>1</sub> (µg m <sup>-3</sup> )	PM <sub>1</sub> Max (µg m <sup>-3</sup> )	Type
E1	Spring	28-30 Apr	M-R <sup>a</sup> /NE <sup>b</sup>	0.7±0.4	41±67	47.1±15.9	25.5±3.1	33.1	LWC
E2	Spring	14-16 May	M-R/NE <sup>b</sup>	1.1±0.8	27±61	38.6±14.5	18.8±6.4	32.4	LWC
E3	Spring	27-29 May	M-R <sup>a</sup> /NE <sup>b</sup>	0.9±0.8	184±263	19.3±9.2	28.4±12.6	64.1	IR
E4	Summer	2 Sep	M-R <sup>a</sup> /NW <sup>b</sup>	0.5±0.4	111±163	20.0±3.1	22.5±6.1	33.7	IR
E5	Summer	20-24 Sep	M-R <sup>a</sup> /NE <sup>b</sup>	2.2±0.5	143±234	14.9±4.6	23.8±4.8	35.9	IR
E6	Autumn	3 Nov	M-R <sup>a</sup> /NE <sup>b</sup>	1.3±0.5	174±271	12.8±5.9	15.6±6.2	30.0	IR
E7	Autumn	13-15 Nov	M-R <sup>a</sup> /NE <sup>b</sup>	1.2±0.5	150±221	19.4±7.0	23.4±7.0	45.2	IR
E8	Winter	24-25 Nov	L-R <sup>a</sup> /NE <sup>b</sup>	1.6±0.5	112±174	14.1±6.6	25.9±6.2	38.6	LRT
E9	Winter	8 Feb	L-R <sup>a</sup> /N <sup>b</sup>	2.2±0.6	49±74	27.8±2.8	29.7±8.1	41.6	LRT
E10	Winter	18-19 Feb	L-R <sup>a</sup> /NE <sup>b</sup>	1.5±0.6	104±170	16.0±5.3	25.5±9.4	64.9	LRT

a: Range of air mass origin: Medium range (M-R); Long range (L-R).

b: Direction of air mass origin: Northeast (NE); Northwest(NW); North (N).

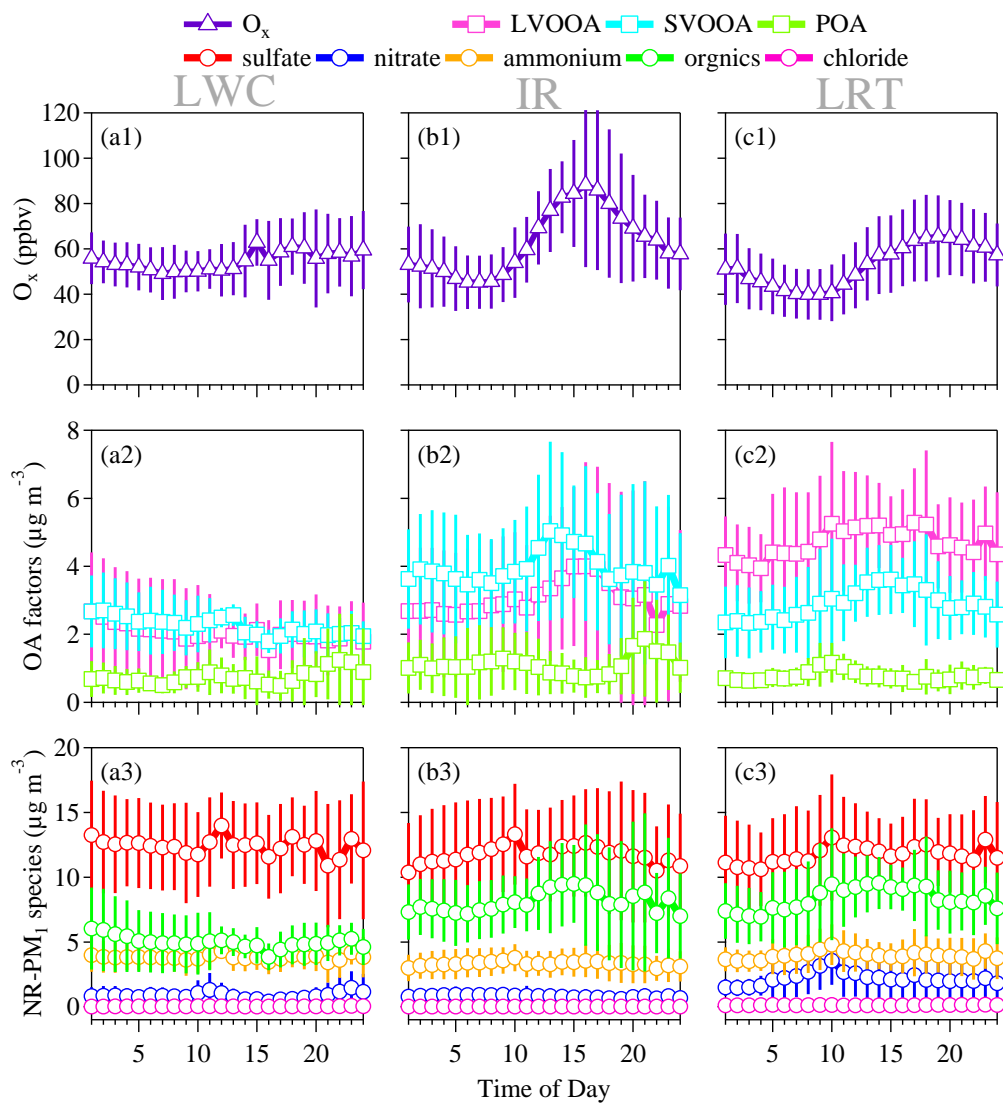


1 **Figures:**



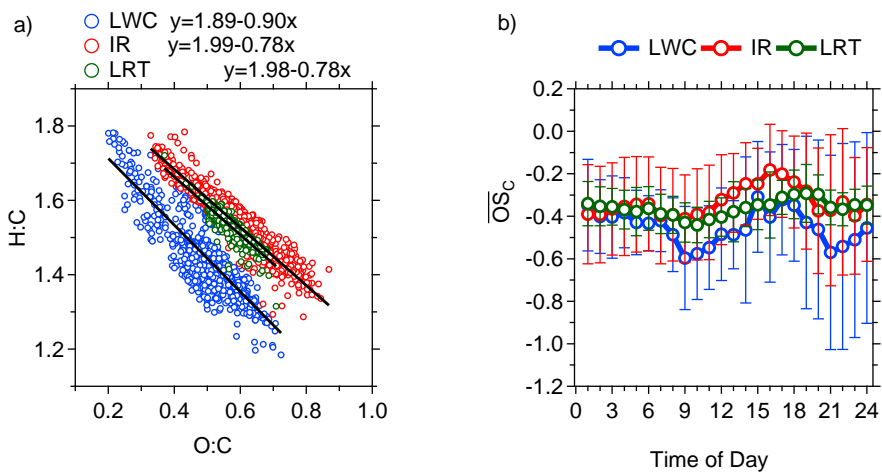
2

3 *Figure 1 Chemical constituents NR-PM<sub>1</sub> in LWC, IR and LRT episodes. (LWC: medium-range transport with high*  
4 *LWC and low IR; IR: medium-range transport with high IR and low LWC; LRT: long-range transport)*



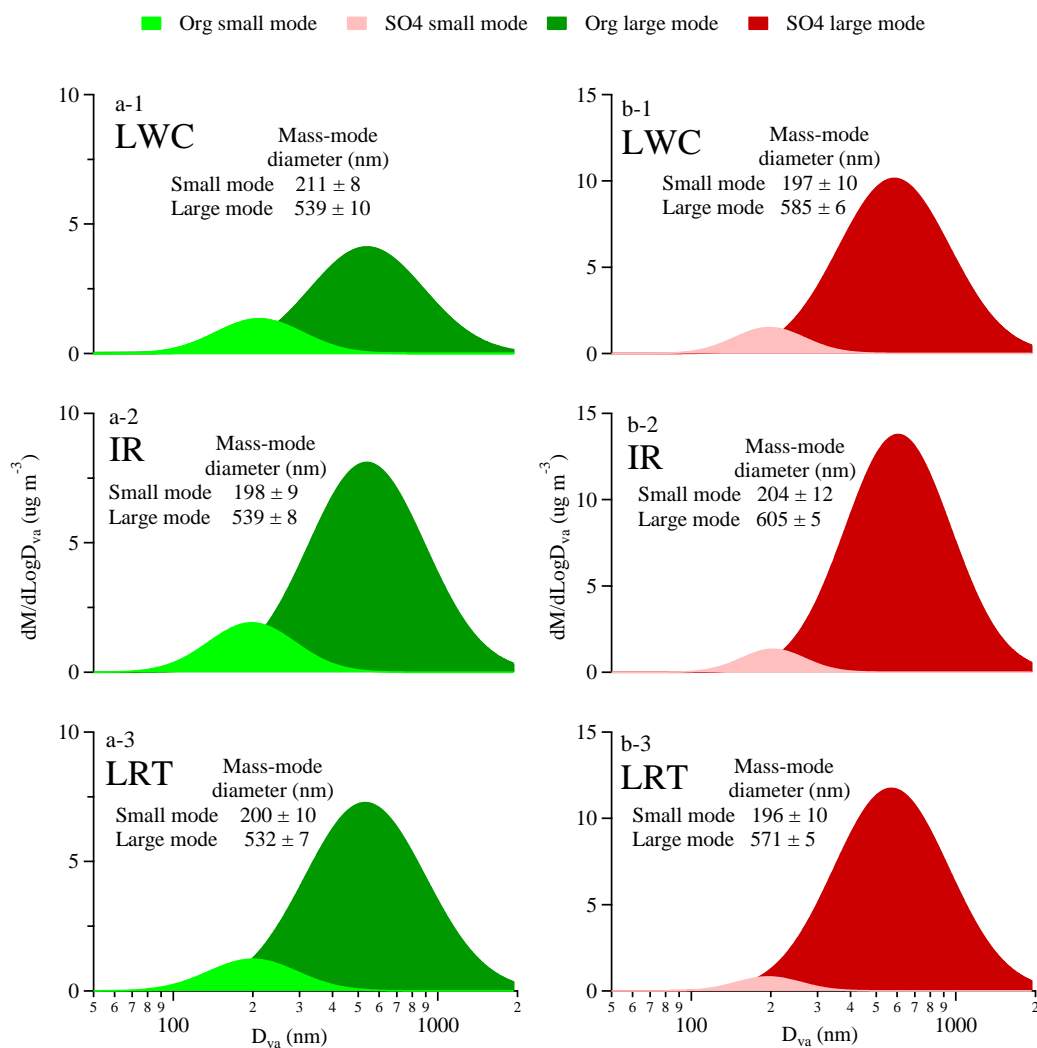
5

6 Figure 2 Summary of diurnal variations of the  $PM_{10}$  species, PMF-resolved organics as well as  $O_3$  in the three types  
 7 of episodes. Means are shown as points and standard deviations are as error bars.



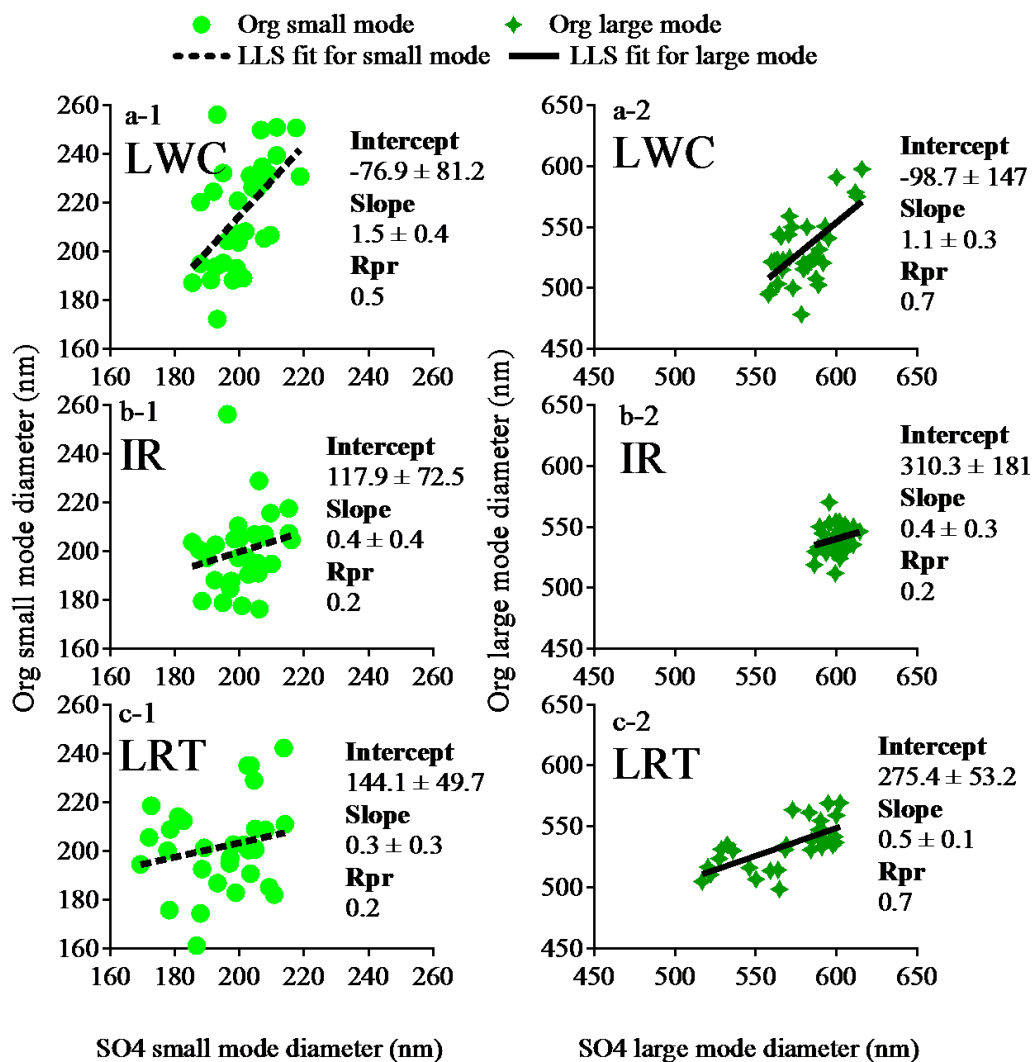
8

9 *Figure 3 a) Van Krevelen diagram for the three types of episodes; b) diurnal variation of carbon oxidation state*  
10 *( $\overline{OS}_c$ ). Means appear as circles with superimposed standard deviations.*



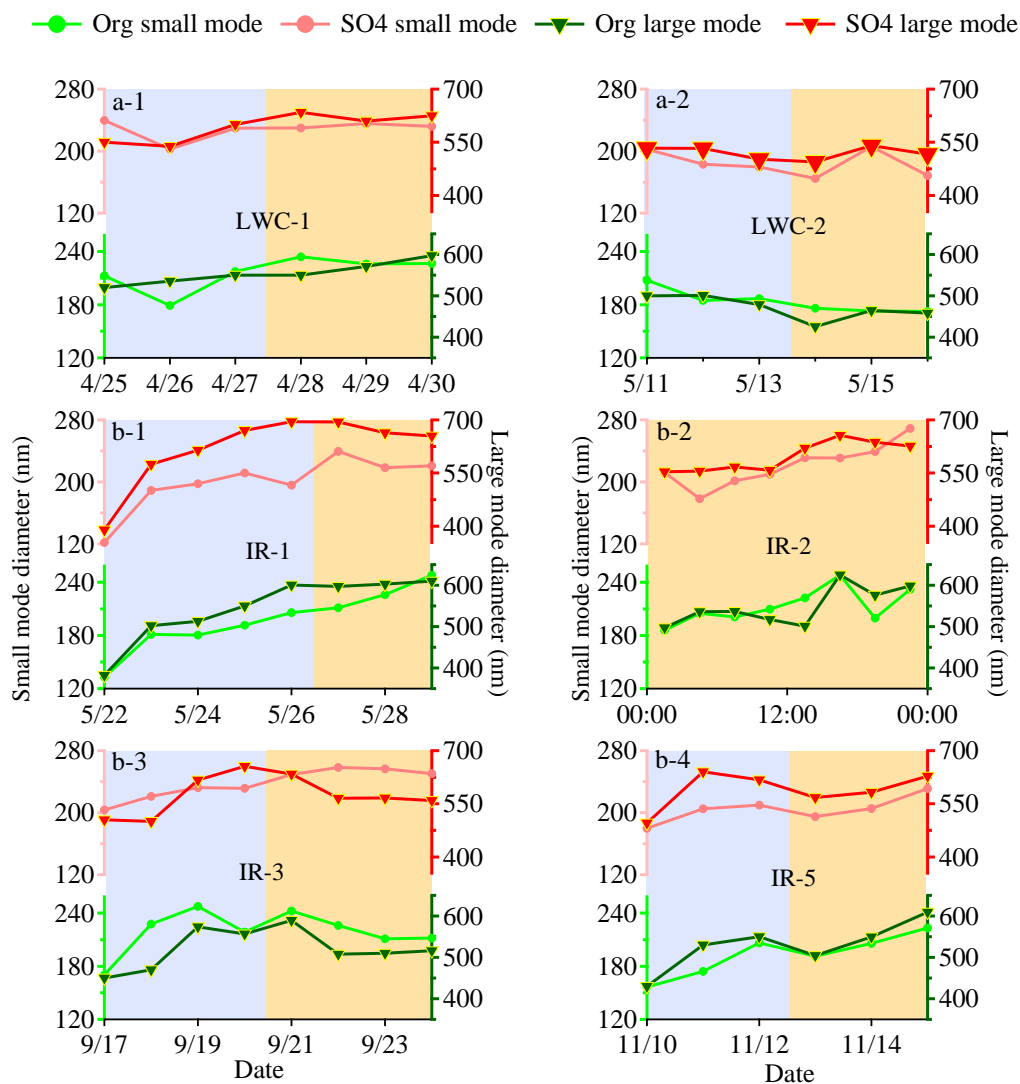
11

12 *Figure 4 Bimodal log-normal fitting results of the size distributions of organics and sulfate during the three types of*  
 13 *episodes. a) Fitted small particle size mode and large particle size mode of organics during LWC, IR and LRT*  
 14 *episodes; b) fitted small particle size mode and large particle size mode of sulfate during LWC, IR and LRT*  
 15 *episodes.*



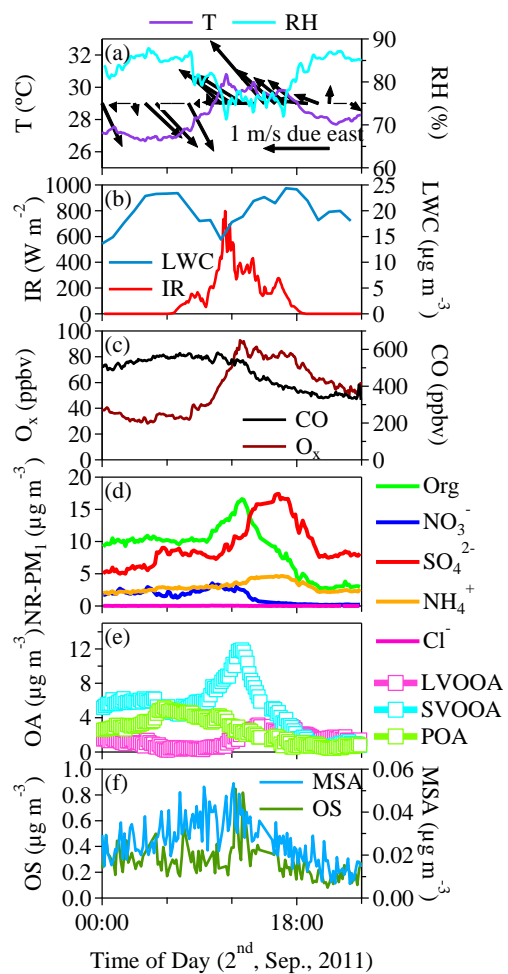
16

17 *Figure 5* Scatter plots and linear least square fits of mass-mode diameters of organics and sulfate during the three  
 18 different types of episodes. a1-a2) small and large mass-mode diameter of organics against sulfate during LWC  
 19 episodes; b1-b2) small and large mass-mode diameter of organics against sulfate during IR episodes; c1-c2) small  
 20 and large mass-mode diameter of organics against sulfate during LRT episodes.



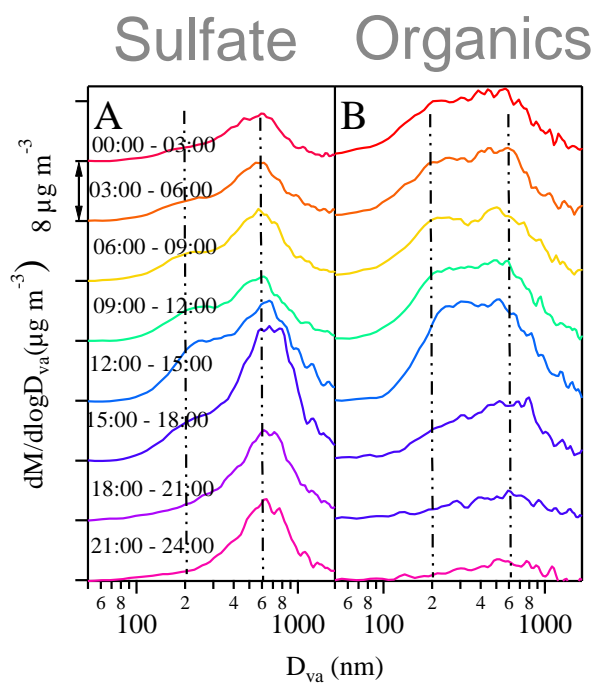
21

22 *Figure 6 Variations of 24-hour averaged size distributions of fitted mass-mode diameters of organics and sulfates*  
 23 *during LWC episodes and IR episodes (shaded in orange) and several days before each episode (shaded in blue).*  
 24 *For the episode that lasted only for a day (E4), 3-hour averaged size distributions of fitted mass-mode diameters are*  
 25 *shown instead. a) LWC episodes; b) IR episodes.*



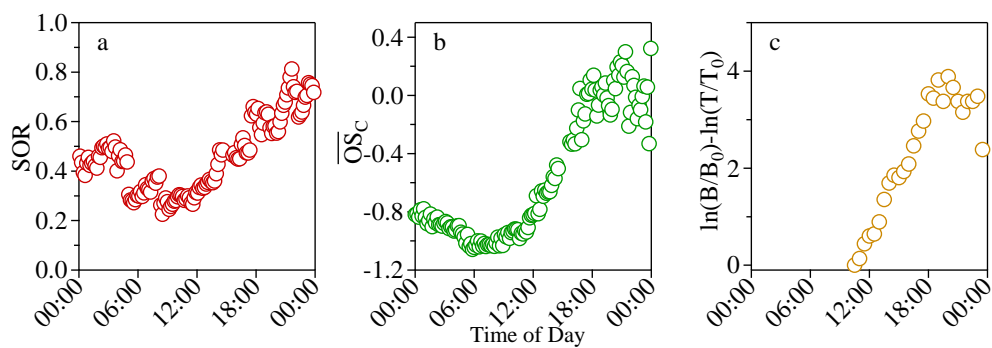
26

27 *Figure 7 Time series of meteorological parameters, gaseous species, NR-PM1 species and PMF-resolved organic*  
 28 *factors in E4.*



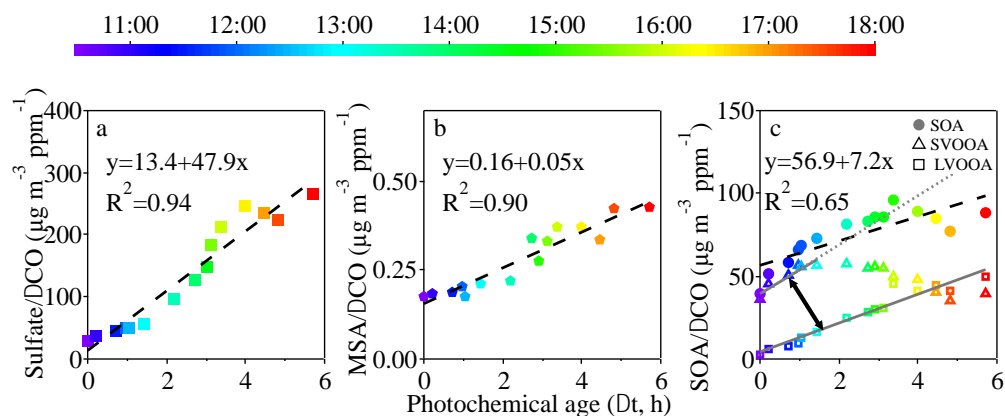
29

30 *Figure 8 Size distributions of sulfate (A) and organics (B) in different time intervals during E4.*



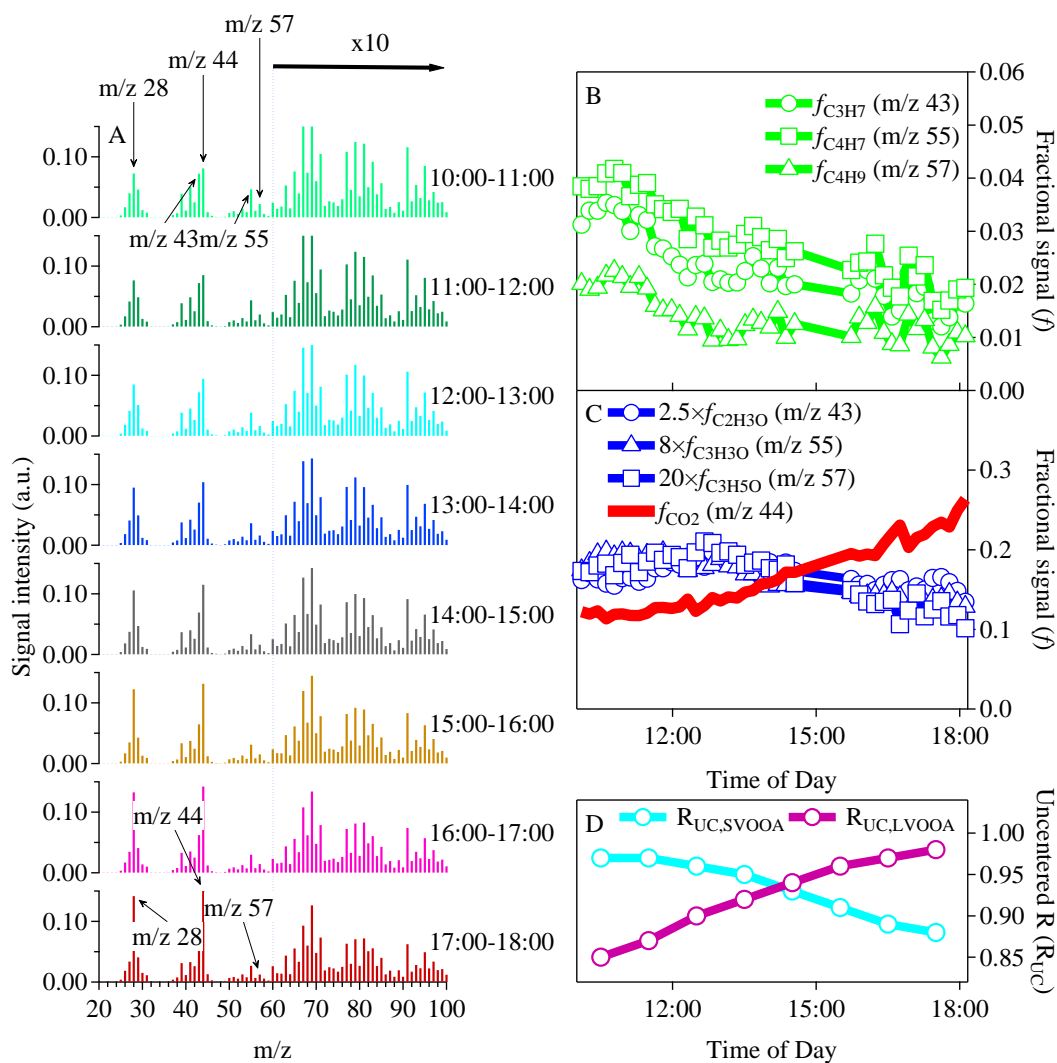
31

32 *Figure 9 Oxidative evolution of aerosol components. a) Sulfur oxidation ratio (SOR); b) average carbon oxidation*  
33 *state  $\overline{OS}_c$ ; c) benzene to toluene ratio ( $B$ : benzene concentration at time  $t$ ;  $B_0$ : benzene concentration at time 0;  $T$ :*  
34 *toluene concentration at time  $t$ ;  $T_0$ : toluene concentration at time 0).*



35

36 *Figure 10 Photochemical production of secondary species. a)  $\Delta\text{CO}$ -normalized sulfate concentration ( $\text{SO}_4/\Delta\text{CO}$ )*  
 37 *as a function of photochemical age; b)  $\Delta\text{CO}$ -normalized MSA concentration ( $\text{MSA}/\Delta\text{CO}$ ) as a function of*  
 38 *photochemical age; and c)  $\Delta\text{CO}$ -normalized secondary organic aerosol concentration ( $\text{SOA}/\Delta\text{CO}$ ,*  
 39  *$\text{SOA}(\text{SVOOA}+\text{LVOOA})$ ) as a function of photochemical age. Data points are colored by time of day. Data points*  
 40 *represent half-hour averages.*



41

42 *Figure 11 Evolution of high-resolution organic mass spectra from 10:00 to 18:00 during the photochemical aging*  
 43 *process in E4: a) mass spectral evolution; b) changes in relative intensities of hydrocarbon-like ions  $C_3H_7^+$  (m/z 43),*  
 44  *$C_4H_7^+$  (m/z 55) and  $C_4H_9^+$  (m/z 57); c) changes in relative intensities of oxygen-containing ions:  $C_2H_3O^+$  (m/z 43),*  
 45  *$C_3H_3O^+$  (m/z 55),  $C_3H_5O^+$  (m/z 57) and  $CO_2^+$  (m/z 44); and c) correlation of OA mass spectra with reference (Mohr et*  
 46 *al., 2012) SVOOA and LVOOA mass spectra.*